Pacific Institute for the Mathematical Sciences
http://www.pims.math.ca
pims@pims.math.ca

The no response test - a sampling method for for inverse scattering problems

D. Russell Luke
PIMS
Simon Fraser University
Burnaby BC V5A 1S6, CANADA

Roland Potthast
Institut for Numerical and Applied Mathematics
University of Göttingen
Germany

Preprint number: PIMS-03-5
Received on March 11, 2003

The no response test - a sampling method for inverse scattering problems

D. Russell Luke[1] and Roland Potthast [2]

Abstract. We describe a novel technique, which we call the no response test, to locate the support of a scatterer from knowledge of a far-field pattern of a scattered acoustic wave. The method uses a set of sampling surfaces and a special test response to detect the support of a scatterer without a priori knowledge of the physical properties of the scatterer. Specifically, the method does not depend on information about whether the scatterer is penetrable or impenetrable nor does it depend on any knowledge of the nature of the scatterer (absorbing, reflecting, etc). In contrast to previous sampling algorithms, the techniques described here enable one to locate obstacles or inhomogeneities from the far field pattern of only one incident field – the no response test is a one-wave-method. We investigate the theoretical basis for the no response test and derive a one-wave uniqueness proof for a region containing the scatterer. We show how to find the object within this region. We demonstrate the applicability of the method by reconstructing sound-soft, sound-hard, impedance and inhomogeneous medium scatterers in two dimensions from one wave with full and limited aperture far-field data.

Key words. inverse problems, scattering theory, image processing

AMS subject classifications. 35R30, 35P25, 68U10, 94A08

1. Introduction. Inverse scattering is concerned with recovering information about a medium and its embedded objects by exciting or illuminating the medium with acoustic or electromagnetic fields and measuring the resulting field. One of the fundamental problems is to determine the location and shape of scatterers that are either buried or located in some inaccessible region of a medium. Applications range from geoscience to medical imaging.

Over the past decade, several innovative and successful methods have been introduced into the area of inverse scattering. Here, we add to the list a methodology that we call the *no response test* and demonstrate its applicability. The idea of the method is to test the hypothesis that a scatterer lies within a given test domain given the far-field data. We sample by construction the set of incident fields that are small on the test domain and large outside. The far-field patterns corresponding to these incident fields are then calculated using the given far-field data. We call the calculated far field patterns *responses*. If all the responses are small, then the unknown scatterer is shown to be a subset of the test domain, that is the hypothesis is true. The unknown scatterer is located within the union of all test domains for which the hypothesis is true. Since small, rather than large, responses indicate the location of the scatterer, the methodology is called the "no response" method.

To place this methodology relative to other reconstruction techniques we give a brief review of the different reconstruction approaches. The evolutionary tree of inverse scattering algorithms is diverse enough that some taxonomy is in order. We separate reconstruction algorithms into three classes: *iterative*, *decomposition*, and *sampling/probe* methods.

[1]Simon Fraser University, Burnaby, British Columbia V5A 1S6, CANADA (luke@cecm.sfu.ca). This author is a Postdoctoral Fellow of the Pacific Institute for the Mathematical Sciences. His work was supported while at the University of Göttingen.

[2]Institut for Numerical and Applied Mathematics, University of Göttingen, Germany; http://www.scienceatlas.de/nfg

Category	Methods
I	**Iterative techniques**
	Newton Method
	Landweber Scheme
	Least Squares Fits (depending on the setup)
	Conjugate Gradient Method
II	**Decomposition techniques**
	Colton-Monk Method / Dual Space Method
	Kirsch-Kress Method
	Potthast / Point Source Method
III	**Probe- and sampling techniques**
	Colton-Kirsch Method / Linear Sampling Method
	Kirsch / Factorization Method
	Potthast / Singular Sources Method
	Ikehata / Probe Method
	Ikehata / Enclosure Method
	Luke-Potthast / No Response Test

Iterative methods (Category I in [16]) use the model of the full forward problem, or an appropriate approximation thereof, for the solution of the inverse problem. These techniques have the advantage that they use all information about the forward problem for the solution of the inverse problem and they usually deliver quite good reconstructions. However, due to the need to solve the forward problem many times, they can be computationally intensive. Also, obtaining a localized reconstruction in a limited data setting is problematic since full data for solving the forward problem is presumed. Indeed, at the very least it is presumed that one knows *which* model the data should satisfy. Well-known examples of iterative techniques are the *Newton method*, the *Landweber method* and various versions of *least-squares fits*.

Decomposition algorithms (Category II in [16]) consist of methods that split the inverse problem into an ill-posed part to reconstruct the scattered field and a well-posed part to find the unknown scatterer due to some boundary condition. Representatives of this type of method are the *dual-space method* proposed by Colton-Monk [3] [4] and the technique of Kirsch-Kress [2], but also newer strategies like the *point source method* of Potthast [16, 14, 15], which turns out to be a type of adjoint method to the Kirsch-Kress technique.

Sampling and probe methods comprise the third and most recent class of algorithms (Category III in [16]). These involve testing a given region with a model mapping the data to a point in the test region and locating the boundary of the unknown scatterer as the points where some unusual or characteristic behavior (usually some resolvable type of blow-up) occurs in the model functions. Where these techniques differ is in the construction of the model functions, which leads to fundamentally different algorithms. These methods share the advantage that they can be applied without knowing whether the scatterer is impenetrable (sound-soft or sound-hard), or an inhomogeneous medium. The no response test belongs to this class. We discuss in more detail the different strategies within this class that have been proposed since 1995.

A scatterer is denoted by its support $\Omega \subset \mathbb{R}^m$ ($m = 2$, or 3) where Ω is bounded. For our purposes we need only assume that the boundary of the scatterer $\partial\Omega$ is Lipschitz, however this introduces mathematical technicalities that cloud the central ideas here. We therefore limit our discussion to twice continuously differentiable (C^2) boundaries. Readers interested in the details of boundaries with corners, or more generally Lipschitz boundaries, are referred to [11, 12]. We denote by $\nu(x_0)$ the *unit outward normal* to Ω at the point $x_0 \in \partial\Omega$, that is, $|\nu(x_0)| = 1$ and the vector product $(y - x_0, \nu(x_0)) \leq 0$ for every $y \in \overline{\Omega}$.

Let $u, u^s : \mathbb{R}^m \to \mathbb{C}$ and $u^\infty : \mathbb{S} \to \mathbb{C}$, denote the *total, scattered*, and *far* fields respectively due to excitation from an *incident plane wave* u^i at a fixed wavenumber $\kappa > 0$. Here $\mathbb{S} := \{x \in \mathbb{R}^m \mid |x| = 1\}$. We parameterize these fields by the *direction of incidence* $\hat{y}$ of the incident plane wave $u^i(x, \hat{y}) := e^{i\kappa x \cdot \hat{y}}$, $x \in \mathbb{R}^m$ $\hat{y} \in \mathbb{S}$, where $i = \sqrt{-1}$ in the exponential. Similarly we write the dependence on the direction of incidence explicitly in the argument of the other fields as $u(x, \hat{y})$, $u^s(x, \hat{y})$, and $u^\infty(\hat{x}, \hat{y})$ respectively. Here and elsewhere, the hat indicates a unit vector, $\hat{x} := \frac{x}{|x|}$. When the far field data is known only on an open subset Γ of $\mathbb{S}$, we call the data *limited aperture* data.

Method	**Amount of far field data needed**	**Assumptions on the physical nature of the scatterer**
Colton-Kirsch / Linear Sampling Method	$u^\infty(\hat{x}, \hat{y})$, $\forall \hat{x}, \hat{y} \in \Gamma \subset \mathbb{S}$	none
Kirsch / Factorization Method	$u^\infty(\hat{x}, \hat{y})$, $\forall \hat{x}, \hat{y} \in \mathbb{S}$	none
Potthast / Singular Sources Method	$u^\infty(\hat{x}, \hat{y})$, $\forall \hat{x}, \hat{y} \in \Gamma \subset \mathbb{S}$	none
Ikehata / Probe Method	$u^\infty(\hat{x}, \hat{y})$, $\forall \hat{x}, \hat{y} \in \mathbb{S}$	none
Ikehata / Enclosure Method	$u^\infty(\hat{x}, \hat{y})$, $\forall \hat{x} \in \mathbb{S}$ *one* $\hat{y} \in \mathbb{S}$	none
Luke-Potthast / No Response Test	$u^\infty(\hat{x}, \hat{y})$, $\forall \hat{x} \in \Gamma \subset \mathbb{S}$, *one* $\hat{y} \in \mathbb{S}$	none

The *linear sampling method* of Colton and Kirsch [1] characterizes the domain of an unknown scatterer by the behavior of the solution to the integral equation of the first kind

$$\int_{\mathbb{S}} u^\infty(\hat{x}, \hat{y}) g(\hat{y}) ds(\hat{y}) = e^{i\kappa \hat{x} \cdot z}, \quad \hat{x} \in \mathbb{S}. \tag{1.1}$$

Here a regularized solution g is calculated for all points z on a sampling grid $\mathcal{G}$. The unknown boundary is found where $||g(z)||$ becomes unbounded.

Kirsch [10] proposed a modified version of this method by constructing a spectral decomposition of the operator

$$(Fg)(\hat{x}) := \int_{\mathbb{S}} u^\infty(\hat{x}, \hat{y}) g(\hat{y}) ds(\hat{y}), \quad \hat{x} \in \mathbb{S},$$

used in (1.1). He proposed to solve the equation

$$(F^* F)^{1/4} g(\hat{x}) = e^{i\kappa \hat{x} \cdot z}, \quad \hat{x} \in \mathbb{S}$$

for all $z \in \mathcal{G}$ and showed that the equation is solvable if and only if z is in the interior of the unknown scatterer. This technique of Kirsch is known as *modified linear sampling* or *factorization method*.

Ikehata and Potthast have independently proposed two related algorithms, the *probe method* [6] and the *method of singular sources* [16] respectively. These techniques are distinct from the (modified) linear sampling methods above in that they use different quantities that blow up when approaching the boundary of some scatterer.

The probe method of Ikehata uses Green's formula to define an indicator function that blows up when the virtual source touches the unknown obstacle. Let Λ be the Dirichlet-to-Neumann map for the boundary value problem in a domain B with the unknown domain $\Omega \subset B$ and Λ_0 be

the Dirichlet-to-Neumann map for B without the existence of Ω. Ikehata proposed to consider

$$I(z,f) := \int_{\partial B} \overline{(\Lambda - \Lambda_0)f} \cdot f ds$$

for specially constructed functions f. It can be shown that $I(z,f)$ tends to infinity if z tends to the boundary of the unknown domain. The Dirichlet-to-Neumann map can be calculated from the far field patterns $u^\infty(\hat{x},\hat{y})$ for all $\hat{x},\hat{y} \in \mathbb{S}$, i.e. from the far field pattern for scattering of all plane waves of one fixed frequency.

The singular sources method of Potthast uses a different functional which also blows up at the boundary of the obstacle. This functional is defined as the magnitude of the *scattered field* $\Psi^s(z,z)$ of singular sources $\Psi(\cdot,z)$ and is calculated by backprojection of the form

$$\Psi^s(y,z) \approx \int_{\mathbb{S}}\int_{\mathbb{S}} u^\infty(\hat{x},\hat{y}) g(\hat{x},y) g(-\hat{y},z) ds(\hat{y}) ds(\hat{x}), \quad y,z \in \mathbb{R}^m \setminus \Omega,$$

for explicitly constructed kernels $g(\cdot,\cdot)$.

All of the linear sampling and probe methods share the advantage that no knowledge about the boundary condition of the unknown scatterer is needed. With the exception of the Kirsch factorization method, these methods are valid in the limited aperture case, where the far field data is not known on the full sphere, but only on an open subset $\Gamma \subset \mathbb{S}$. The principle disadvantage of sampling and probe techniques, however, is that they all require the knowledge of far field patterns for a large number of incident plane waves. The current challenge facing these algorithms is to reduce the amount of data needed for reliable reconstructions.

Recent work by Ikehata has made significant progress toward the development of reconstruction algorithms using very limited data. His *enclosure method* [7, 8] enables one to find the support of convex polygons from the knowledge of one measured field. Ikehata uses a special harmonic incident field

$$v = e^{\tau x \cdot (\omega + i\omega^\perp)},$$

to construct the following indicator function

$$I_\omega(\tau,t) = e^{-\tau t}\left\{ \left\langle \left.\frac{\partial u}{\partial \nu}\right|_{\partial G}, v|_{\partial G} \right\rangle - \left\langle \left.\frac{\partial v}{\partial \nu}\right|_{\partial G}, u|_{\partial G} \right\rangle \right\}, \quad \tau > 0, \quad t \in \mathbb{R}, \tag{1.2}$$

where $\omega \in \mathbb{S}$ is a direction vetor, u is the unknown, weak solution to the scattering problem and G is some domain containing the unknown scatterer, $\Omega \subset \operatorname{int} G$ the interior of G. Ikehata shows that at the corners of polygonal scatterers this indicator function becomes unbounded. He then exploits this property to uniquely reconstruct the scatterer. For details on implementation see [9]. While for the purposes of analysis the presentation of the enclosure method is limited to specific settings, it appears that in practice the method is independent of the material properties of the scatterer.

In this work we propose another technique for locating a scatterer from a single incident wave that also exploits the behavior of a special indicator function in the neighborhood of a scatterer. Since we look, rather, for where the indicator function does *not* become unbounded, we call the method the no response test. Like the enclosure method, the no response test can be used to locate scatterers from only one incident wave. Moreover, neither the enclosure method nor the no response test require a priori knowledge of the material properties of the scatterer. However, the indicator function in the no response test is a different functional on the measured data than that of Ikehata. Also, we do not make use of, nor place any particular constraints on, the goemetric properties of the scatterer.

It is often the case that numerical algorithms preceed by many years their mathematical justification. The absence of analytical results for a particular application does not preclude the successful implementation and numerical study of algorithms. At the expense of mathematical analysis limited to narrow settings, we have chosen to highlight the robustness of the no response test in a variety of settings by focusing on numerical results. We leave many unanswered questions, however the demonstration of the applicability of the techniques discussed here helps to motivate and formulate the analysis that must follow. In Section 3 we provide preliminary theoretical results to motivate the method. A convergence proof for one-wave reconstructions would include a one-wave uniqueness result. These results are not yet available. However, we can show that a set (depending on some test domain Ω_t^0) surrounding the unknown scatterer, which we call its *corona*, is uniquely determined by the one-wave far field pattern independent of the boundary condition.

The no response algorithm is given in Section 4. In the same section we show reconstructions for scattering from scatterers with *Dirichlet*, *Neumann*, or *impedance* boundary condition, or for scattering from an inhomogeneous medium. We show results from each of these scatterers with full and limited aperture data. Preparatory to this, we briefly review in Section 2 the fundamental scattering models for sound-soft, sound-hard, and mixed obstacles as well as inhomogeneous media.

2. Dirichlet, Neumann, impedance and medium scattering problems. This section serves to briefly review the key elements of scattering by bounded objects or media, and to provide some tools for the inversion method described in Section 3. We also describe how we solved the forward problems to produce the data used for the demonstration of the no response test.

Scattering review. Let v^i be an incident field that satisfies the Helmholtz equation,

$$\triangle v + \kappa^2 v = 0,$$

with wave number $\kappa > 0$ on $\mathbb{R}^m$. The incident field produces a scattered field v^s that solves the Helmholtz equation on the exterior of the scatterer Ω and satisfies the *Sommerfeld radiation condition*

$$r^{\frac{m-1}{2}}\Big(\frac{\partial}{\partial r} - i\kappa\Big)v(x) \to 0, \quad r = |x| \to \infty$$

uniformly in all directions. For impenetrable scatterers we consider cases where the scatterer is either sound-soft (a perfect conductor), sound-hard (a perfect reflector) or some mixture of these. Each of these types of scatterers is modeled by a total field,

$$v = v^i + v^s,$$

that satisfies either *Dirichlet, Neumann* or *impedance* boundary conditions. These boundary conditions are given respectively as

$$v|_{\partial\Omega} = 0, \qquad \frac{\partial v}{\partial \nu}|_{\partial\Omega} = 0, \qquad \frac{\partial v}{\partial \nu}|_{\partial\Omega} + \lambda v|_{\partial\Omega} \;=\; 0,$$

with the impedance function $\lambda \in C(\partial\Omega)$. We also treat penetrable scatterers, where the inhomogeneity is modeled by a nonegative refractive index $n : \mathbb{R}^m \to \mathbb{R}_+$ and where $n(x) := 1$ for $x \in \mathbb{R}^m \setminus \Omega$. Then the total field $v \in H^2_{loc}(\mathbb{R}^m)$ solves the inhomogeneous Helmholtz equation,

$$\triangle v + \kappa^2 n v = 0,$$

in $\mathbb{R}^m$, and $v^s = v - v^i$ satisfies the Sommerfeld radiation condition.

The following result enables us to calculate the scattered and far fields of any reasonable incident field as the weighted superposition of the corresponding fields generated by scattering from incident plane waves. This result is fundamental to the no response test.

THEOREM 2.1. *Let Γ be an open subset of $\mathbb{S}$, the unit sphere on $\mathbb{R}^m$ ($m = 2, 3$), and let $\Omega \subset \mathbb{R}^m$ denote the bounded support of a scattering body with C^2 boundary. Denote by $u^s : \mathbb{R}^m \to \mathbb{C}$ and $u^\infty : \mathbb{S} \to \mathbb{C}$, the scattered and far fields respectively due to excitation from an incident plane wave u^i at a fixed wavenumber $\kappa > 0$ with direction $-\hat{y}$, $u^i(x, -\hat{y}) := e^{i\kappa x\cdot(-\hat{y})}$, $x \in \mathbb{R}^m$, $\hat{y} \in \mathbb{S}$. Consider the superposition of plane waves*

$$v^i(x) = \int_\Gamma e^{i\kappa x\cdot(-\hat{y})} g(-\hat{y}) ds(\hat{y}), \quad x \in \mathbb{R}^m, \tag{2.1}$$

where $g \in L^2(-\Gamma)$. The corresponding solution to the scattering problem with Dirichlet, Neumann or impedance boundary conditions or scattering by an inhomogeneous medium is given by $v = v^i + v^s$ where

$$v^s(x) = \int_\Gamma u^s(x, -\hat{y}) g(-\hat{y}) ds(\hat{y}), \quad x \in \mathbb{R}^m \setminus \overline{\Omega}.$$

The corresponding far field pattern is given by

$$v^\infty(\hat{x}) = \int_\Gamma u^\infty(\hat{x}, -\hat{y}) g(-\hat{y}) ds(\hat{y}), \quad \hat{x} \in \mathbb{S}. \tag{2.2}$$

Proof. The proof relies only on the linearity and boundedness of the particular scattering problem. Linearity implies that the sum of two incident fields is scattered onto the sum of the single scattered fields. By boundedness of the scattering operator from $C(\Omega)$ into $C_{loc}(\mathbb{R}^m \setminus \overline{\Omega})$ the limit for the integration can be performed and we obtain the stated results. □

The signs in the expressions for v^i, v^s, and v^∞ above have been chosen so that the backprojection mapping between the far field measurments and the scattered field which we derive below has a natural interpretation in terms of a physical aperture in the far field. Note that the function g is defined on $-\Gamma$ where $-\Gamma$ is the mirror image of the interval Γ: $\hat{y} \in \Gamma \iff -\hat{y} \in -\Gamma$. Using the standard far field reciprocity relation $u^\infty(\hat{x}, -\hat{y}) = u^\infty(\hat{y}, -\hat{x})$, $(\hat{x}, \hat{y} \in \mathbb{S})$, we see that the far field is defined on Γ with any incident wave direction $-\hat{x}$. When $\Gamma = \mathbb{S}$ this virtual aperture is not as apparent. The incident field v^i given by Eq.(2.1) is called a *Herglotz wave function*. Since this function depends on the density g we write this explicitly as $v^i[g](x)$. We denote the scattered field for scattering of a Herglotz wave function $v^i[g](x)$ by $v^s[g](x)$. Similarly the corresponding far field pattern is given by $v^\infty[g](\hat{x})$.

Numerical considerations. As a basis both for the theoretical discussion and the implementations (that is, the generation of the simulated data) we briefly sketch the solution of the above scattering problems. For all proofs and a detailed discussion we refer to [2] and [16].

For the solution of the Dirichlet problem we represent the scattered field as a combined single- and double layer potential

$$v^s(x) = \int_{\partial\Omega} \left\{ \frac{\partial\Phi(x, y)}{\partial\nu(y)} - i\Phi(x, y) \right\} \varphi(y) ds(y), \quad x \in \mathbb{R}^m \setminus \partial\Omega.$$

For this representation of the scattered field and the boundary condition, the density φ must satisfy the integral equation

$$\varphi + K\varphi - iS\varphi = -2v^i, \tag{2.3}$$

where $\mathcal{S}$ is the single-layer operator,

$$(S\varphi)(x) := 2\int_{\partial\Omega} \Phi(x,y)\varphi(y)ds(y), \quad x \in \partial\Omega$$

and K is the double-layer operator,

$$(K\varphi)(x) := 2\int_{\partial\Omega} \frac{\partial\Phi(x,y)}{\partial\nu(y)}\varphi(y)ds(y), \quad x \in \partial\Omega.$$

The equation has a unique solution that depends continuously on the right-hand side in $C(\partial\Omega)$.

For the Neumann problem we use the modified approach due to Panich [13]

$$v^s(x) = \int_{\partial\Omega} \left\{ \Phi(x,y)\varphi(y) + i\frac{\partial\Phi(x,y)}{\partial\nu(y)}(S_0^2\varphi)(y) \right\} ds(y), \quad x \in \mathbb{R}^m \setminus \partial\Omega, \tag{2.4}$$

where S_0 denotes the single layer operator in the case $\kappa = 0$. For this representation of the scattered field, the density φ can be shown to satisfy the boundary integral equation

$$\varphi - K'\varphi - iTS_0^2\varphi = 2\frac{\partial v^i}{\partial\nu} \tag{2.5}$$

where

$$(K'\varphi)(x) := 2\int_{\partial\Omega} \frac{\partial\Phi(x,y)}{\partial\nu(x)}\varphi(y)ds(y), \quad x \in \partial\Omega,$$

and

$$(T\varphi)(x) := 2\frac{\partial}{\partial\nu(x)}\int_{\partial\Omega} \frac{\partial\Phi(x,y)}{\partial\nu(y)}\varphi(y)ds(y), \quad x \in \partial\Omega.$$

Both Eq.(2.3) and Eq.(2.5) have unique solutions that depend continuously on the incident field in $C(\partial\Omega)$.

For the impedance boundary value problem we follow the same approach using the representation (2.4). An application of the jump relations leads to the equation

$$\left[I - K' - iTS_0^2 - \lambda S - i\lambda(I+K)S_0^2\right]\varphi = 2\frac{\partial v^i}{\partial\nu} + 2\lambda v^i. \tag{2.6}$$

Under suitable assumptions on the impedance λ (basically ensuring uniqueness of the impedance scattering problem) the integral equation Eq.(2.6) has a unique solution which depends continuously on the incident field in $C(\partial\Omega)$.

For the penetrable inhomogeneous medium we use Green's formula applied to the total field to recast the solution to the scattering problem as the solution to the *Lippmann-Schwinger* equation

$$v(x) \;=\; v^i - \kappa^2 \int_{\mathbb{R}^m} \Phi(x,y)m(y)v(y), \quad x \in \mathbb{R}^m,$$

where $m(y) := 1 - n(y)$ for the index of refraction $n : \mathbb{R}^m \to \mathbb{R}_+$. The Lippmann-Schwinger equation has a unique solution in $C(\Omega)$ that depends continuously on the incident field v^i.

3. The inverse problem and the no response test. The *inverse problem* we consider is to locate the scatterer Ω given an incident plane wave u^i and the far field data restricted to the aperture $u^\infty|_\Gamma$, where $\Gamma \subset \mathbb{S}$ is some open set. The solution to the inverse problem is often called the *reconstruction* of the scatterer. The no response method is a reconstruction algorithm that uses only one incident wave, and does not use any a priori information about the physical characteristics of the scatterer.

We consider the hypothesis that a scatterer lies within a given domain. The no response test is a way to determine whether or not this hypothesis is true. We begin with a heuristic description of the reconstruction method based on this test. An explicit formulation of the full algorithm is given in the next section.

The scattering test response. Let $\Omega_t \subset \mathbb{R}^m$ be a bounded test domain with a C^2 boundary. Sample by construction (see Eq.(2.1)) the set of incident fields that are small on the test domain Ω_t and large outside. The far-field patterns corresponding to these incident fields are then calculated via Eq.(2.2). We call the magnitude of the calculated far field patterns *responses*. If the maximum of the sampled responses is small, we show that this is an indication that the unknown scatterer is a subset of the test domain Ω_t. While general goemetric properties of the test domain are not important (e.g. convexity, symmetry, and so forth), it is critical that the test domain be large enough that by translation the scatterer is containted in the interior. The no response algorithm makes use of a template test domain Ω_t^0 that is rotated and translated around the computational domain. The location and shape of the scatterer is then recovered by the behavior, with respect to these test domains, of the sampled *scattering test response*, that is, the supremum over all responses for a fixed test domain. This is defined below.

DEFINITION 3.1 (scattering test response). *Given the far field pattern u^∞ due to an incident plane wave u^i with direction $-\hat{x}$ and a scatterer Ω as in Theorem 2.1, let $v^i[g]$ denote a Herglotz wave function defined by Eq.(2.1), and $v^\infty[g]$ the corresponding far field pattern given by Eq.(2.2). We define the* scattering test response *for the test domain Ω_t by*

$$\mu_\epsilon(\Omega_t, \Omega, \hat{x}) := \sup\left\{ |v^\infty[g](\hat{x})| : \quad g \in L^2(-\Gamma) \right. \\ \left. \text{such that } ||v^i[g]||_{C(\Omega_t)} \leq \epsilon \right\}. \tag{3.1}$$

We keep the direction $\hat{x}$ fixed in the sequel, so to reduce notational clutter we drop the argument and use the notation $\mu_\epsilon(\Omega_t, \Omega)$ whenever there is no chance for confusion.

To calculate μ_ϵ from the far field pattern $u^\infty|_\Gamma$ for scattering of a plane wave u^i with direction $-\hat{x}$, we use the reciprocity relation $u^\infty(\hat{x}, -\hat{y}) = u^\infty(\hat{y}, -\hat{x})$, $(\hat{x}, \hat{y} \in \mathbb{S})$ and Theorem 2.1 to obtain

$$\begin{aligned} v^\infty(\hat{x}) &= \int_\Gamma u^\infty(\hat{x}, -\hat{y}) g(-\hat{y}) ds(\hat{y}) \\ &= \int_\Gamma u^\infty(\hat{y}, -\hat{x}) g(-\hat{y}) ds(\hat{y}). \end{aligned} \tag{3.2}$$

Thus, from knowledge of the far field pattern $u^\infty(\hat{y}, -\hat{x}),\ \hat{y} \in \Gamma$ for one wave with direction of incidence $-\hat{x}$, we can reconstruct $\mu_\epsilon(\Omega_t, \Omega)$ for any domain Ω_t by construction of appropriate kernels g of the (limited aperture) Herglotz wave functions. Before discussing in detail the construction of the densities g and the test domains Ω_t, we prove some basic results about the behavior of the scattering test response that motivate our numerical methods.

The no response test is built upon two observations. First, when the scatterer Ω is contained in *interior* of the test domain Ω_t, the value $\mu_\epsilon(\Omega_t, \Omega)$ is *small or bounded*. Second, if the scatterer is in the *exterior* of the test domain then $\mu_\epsilon(\Omega_t, \Omega)$ *large or unbounded*. These facts are used to locate the support Ω of the scatterer as a region contained in the union of test domains where

the scattering test response μ_ϵ is bounded. We summarize this critical behavior in the following theorem.

THEOREM 3.2 (behavior of the scattering test response). *If $\Omega \subset \Omega_t$ then there is a constant $c \in \mathbb{R}$ such that*

$$\mu_\epsilon(\Omega_t, \Omega) \leq c\epsilon.$$

On the other hand, if $\overline{\Omega} \cap \overline{\Omega}_t = \emptyset$, and $\mathbb{R}^m \setminus (\overline{\Omega} \cup \overline{\Omega}_t)$ is connected, then we have

$$\mu_\epsilon(\Omega_t, \Omega) = \infty.$$

Proof. When $\Omega \subset \Omega_t$ the boundedness of the scattering map $v^i \mapsto v^\infty$ implies the existence of a constant c such that for all v^i satisfying

$$||v^i||_{C(\Omega_t)} \leq \epsilon,$$

we have

$$||v^\infty||_{C(\mathbb{S})} \leq c\epsilon.$$

This completes the proof of the first statement.

To prove the second statement, we consider two disjoint domains, Ω_t' and Ω' satisfying $\Omega_t \subset \Omega_t'$, $\Omega \subset \Omega'$ and $\overline{\Omega_t'} \cap \overline{\Omega'} = \emptyset$. We further require that the interior homogeneous Dirichlet problems for Ω_t' and Ω' have only the trivial solution. Then the Herglotz wave operator $H : L^2(-\Gamma) \to L^2\Big(\partial(\Omega_t' \cup \Omega')\Big)$, defined by

$$(Hg)(x) := v^i[g](x)\Big|_{\partial(\Omega_t' \cup \Omega')},$$

has dense range. This can be shown in a similar fashion to the proof of Lemma 3.1.2 of [16]. Choose $y \notin \overline{\Omega_t'} \cup \overline{\Omega'}$ such that the far field pattern $w^\infty(\hat{x}, y)$ for scattering of $\Phi(\cdot, y)$ by Ω is not zero. This is always possible since, by the mixed reciprocity relation ([16, Theorem 2.1.4]), we have

$$w^\infty(\hat{x}, y) = \gamma u^s(y, -\hat{x})$$

and $u^s(\cdot, -\hat{x})$ cannot vanish on an open subset of $\mathbb{R}^m$. Next, construct $v^i[g](x)$ satisfying

$$||v^i[g](x)||_{C(\Omega_t')} \leq \epsilon, \;\; ||v^i[g](x) - \beta\Phi(\cdot, y)||_{C(\Omega')} \leq \epsilon.$$

Then since $\Omega_t \subset \Omega_t'$, we have

$$\mu_\epsilon(\Omega_t, \Omega) \geq |v^\infty[g](\hat{x})|.$$

By definition $\Omega \subset \Omega'$, thus

$$\Big|v^\infty[g](\hat{x}) - \beta w^\infty(\hat{x}, y)\Big| \leq c\epsilon,$$

with some constant c, which, by the triangle inequality, yields

$$|v^\infty[g](\hat{x})| \geq \beta|w^\infty(\hat{x}, y)| - c\epsilon.$$

Thus we have

$$\mu_\epsilon(\Omega_t, \Omega) \geq \beta|w^\infty(\hat{x}, y)| - c\epsilon,$$

for all $\beta \in \mathbb{R}$. This completes the proof. □

REMARK 3.3. *In general we would like to know if the implication*

$$\Omega \not\subset \Omega_t \implies \mu_\epsilon(\Omega_t, \Omega) = \infty$$

is true. It would immediately yield a convergence proof of the no response test to find the support of unknown scatterers. This implication is strongly linked to the uniqueness question for the inverse scattering problem under consideration, for which to date there is no proof. Colton and Sleeman [5] have proven uniqueness for the problem with Dirichlet boundary data given a finite number of incident fields and a priori information about the size of the scatterer. The number of incident fields required depends on the size of the scatterer and the wavelength of the incident field. Alternatively, we could try to prove

$$\Omega \not\subset \Omega_t \implies \mu_\epsilon(\Omega_t, \Omega) > C$$

for the smallest constant $C = c\epsilon$ for which Theorem 3.2 is true. This would also lead to a convergence proof for the no response test under the condition that the right constant C is chosen appropriately for the judgment about a test domain. Both problems will be part of future research.

In the following corollary to Theorem 3.2, we use Eq.(3.2) to show that the far field pattern on a limited aperture Γ resulting from excitation by a single incident field uniquely determines the union of all translations of a fixed test domain Ω_t^0 for which μ_ϵ is finite. This is stated precisely below.

DEFINITION 3.4 (corona of Ω corresponding to Ω_t^0). *Let Ω_t^0 denote a fixed, bounded test domain with C^2 boundary. Denote translations of Ω_t^0 by $\Omega_t^0(z) := \Omega_t^0 + z$ for $z \in \mathbb{R}^m$. Define the* corona *of the scatterer Ω by*

$$M(\Omega_t^0, \Omega, \hat{x}) := \bigcup \{\Omega_t^0(z) : \ z \in \mathbb{R}^m, \mu_\epsilon(\Omega_t^0(z), \Omega, \hat{x}) < \infty\}. \tag{3.3}$$

COROLLARY 3.5 (uniqueness and bounds for the corona). *Let $\Omega_t^0 \subset \mathbb{R}^m$ with $\mathbb{R}^m \backslash \overline{\Omega_t^0}$ connected be a bounded domain large enough that there is some $z \in \mathbb{R}^m$ for which $\Omega \subset \Omega_t^0(z)$, where Ω denotes the support of the scatterer. Then we have*

$$M(\Omega_t^0, \Omega, \hat{x}) \subset \bigcup \left\{\Omega_t^0(z) : \ z \in \mathbb{R}^m, \overline{\Omega_t^0}(z) \cap \overline{\Omega} \neq \emptyset\right\} \tag{3.4}$$

and the scatterer Ω is a subset of its corona, $M(\Omega_t^0, \Omega, \hat{x})$. Moreover, the corona is uniquely determined by the far field pattern for scattering of one plane wave with direction of incidence $-\hat{x}$.

Proof. For points z with $\mu_\epsilon(\Omega_t^0(z)) < \infty$,, we apply Theorem 3.2 to conclude that $\overline{\Omega_t^0}(z) \cap \overline{\Omega} \neq \emptyset$, from which we immediately obtain the relation (3.4). For $\Omega \subset \Omega_t^0(z)$ we have $\mu_\epsilon(\Omega_t^0(z)) < \infty$ and thus the support of the scatterer is a subset of its corona: $\Omega \subset M$.

Using Eq.(3.2) the values of $\mu_\epsilon(\Omega_t^0(z), \Omega, \hat{x})$ can be calculated directly from the limited aperture far field pattern $u^\infty(\hat{y}, -\hat{x})$, $\hat{y} \in \Gamma$, that is, for fixed test domain Ω_t^0 and direction $\hat{x}$, the scattering test response $\mu_\epsilon(\Omega_t^0(z), \Omega, \hat{x})$ is a scalar-valued mapping of $\hat{x}$. Since the direction of incidence of a plane wave uniquely determines the far field pattern $u^\infty(\cdot, -\hat{x})$, then the corona is uniquely determined by the far field pattern u^∞. □

The corona corresponding to the circular test domain of a boat-shaped scatterer (see Figure 3.1) is shown in Figure 3.2. From the above uniqueness theorem we know that the unknown

scatterer – whatever its physical nature might be – is located in the corona. Note that, at the very least, we can use the center of the corona for a single incident wave as an estimate for the center of the obstacle. In our experiments here, however, we are able to extract even more information about the scatterer from the corona. Recall from Remark 3.3 that we cannot say anything specific about the behavior of μ_ϵ for $\overline{\Omega} \cap \overline{\Omega_t^0}(z) \neq \emptyset$ when $\Omega \not\subset \Omega_t^0(z)$. We observe numerically that the value of the scattering test response increases as the intersection $\overline{\Omega} \cap \overline{\Omega_t^0}(z) \neq \emptyset$ becomes smaller. We therefore propose a technique that allows us to detect these increases, and thereby detect the location and shape of the scatterer within the corona. We begin by describing the choice of the test domain and the calculation of the scttering test response. Details for efficient implementation together with the algorithm are given in the following section.

The test domain Ω_t^0. For fixed scatterers Ω and incident wave directions $\hat{x}$, the scattering test response μ_ϵ takes as input the test domains $\Omega_t^0(z)$ and returns a scalar value as output. We would like to know which test domains $\Omega_t^0(z)$ yield small values for μ_ϵ without having to work with the unwieldy domains themselves. For this, we construct a mapping from the domain $\Omega_t^0(z)$ to the point $z' \in \Omega_t^0(z)$ and assign to that point the corresponding value of μ_ϵ. It is how we choose the point z' that allows us to get much more information about the obstacle than we would expect.

The key property that we exploit is the observation that μ_ϵ grows as the intersection $\Omega \cap \Omega_t^0(z)$ becomes smaller. We emphasize that this observation is *empirical*, since at this time we cannot prove anything about the behavior of μ_ϵ in this situation. In order to detect this growth, assign the domain $\Omega_t^0(z)$ to a point z' on the *boundary* $\partial\Omega_t^0(z)$. To avoid keeping track of more points than necessary, we construct the generating domain Ω_t^0 such that $0 \in \partial\Omega_t^0$ and map the translated domain $\partial\Omega_t^0(z)$ to the point $z' = z$. When $z \in \Omega$ then the the scatterer will not to fall entirely within the domain $\Omega_t^0(z)$. In this case we observe that the scattering test response μ_ϵ is significantly higher than when z is in the parts of the corona that do not intersect with the scatterer, representing the situation where $\Omega \subset \Omega_t^0(z)$.

We now describe a special realization of the no response test. We assign to the point z the value of the scattering test response

$$f^*(z; \Omega_t^0) := \mu_\epsilon(\Omega_t^0(z), \Omega). \tag{3.5}$$

However, by restriction to the point z from the full set $\overline{\Omega_t^0}(z)$ we loose information: we obtain small values for $f^*(z; \Omega_t^0)$ only on one side of the unknown object as shown in Figure 3.3, where $f^*(z; \Omega_t^0)$ is plotted. The full information is recovered by rotating the generating domain Ω_t^0 around the origin and repeating the above procedure. This is described in detail next.

Rotations or other variations of the test domain are necessary because of our choice of the mapping from $\Omega_t^0(z)$ to the point $z' \in \Omega_t^0(z)$. Had we chosen a radially symmetric generating domain Ω_t^0 and mapped this domain to its center, rotations would not be necessary. However, in this case the image does not directly reflect the behavior of the test response that we use to reconstruct the obstacle, not just its corona, that is, the behavior of the test response when the boundary of the test domain intersects the scatterer. Note that the idea of monitoring the behavior at the boundary of the test domain also appears in the enclosure method, where the test domain is a half-space and the behavior of the indicator function Eq.(1.2) indicates which half-space the obstacle belongs to [6, 9]. Alternatively, we could use an arbitrary set of generating domains Ω_t^0 with $0 \in \partial\Omega_t^0$, however it is much more convenient to work with a single generating domain rotated about the origin.

The value $f^*(z; \Omega_t^0)$ assigned to the point z via Eq.(3.5) at one rotation of the domain Ω_t^0 does not necessarily correspond to the value of the same point at a different rotation. To see this, suppose that the scatterer Ω is contained in a small circle of radius 1 centered at the point $(-1, 0)$. Suppose further that Ω_t^0 is a circle of radius 2 with center $(-2, 0)$. In this case $\Omega \subset \Omega_t^0$ and $f^*(0; \Omega_t^0)$ will therefore be small. If we rotate Ω_t^0 about the origin by 180° and denote the

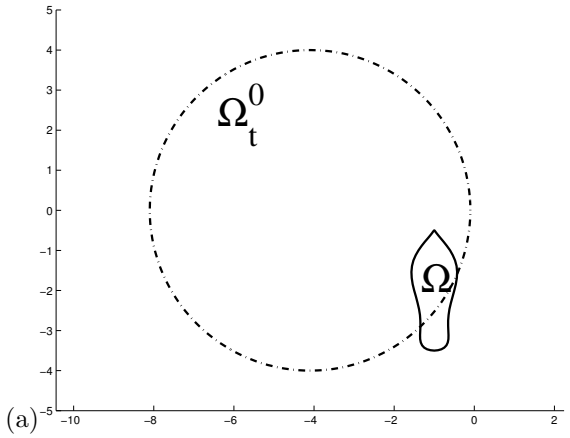

(a)

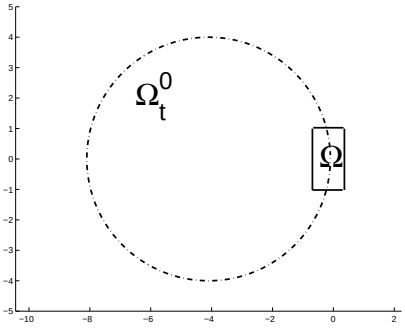

(b)

FIG. 3.1. *Scatterer Ω, and test domain Ω_t^0 used in reconstruction simulations. The obstacle Ω in (a) is used for Dirichlet, Neumann and impedance obstacle reconstructions. The scatterer shown in (b) is used for inhomogeneous media reconstructions.*

resulting domain by $\widetilde{\Omega_t}^0$, then $\Omega \cap \widetilde{\Omega_t}^0 = \{0\}$. In this case we observe that the corresponding value for $f^*(0; \widetilde{\Omega_t}^0)$ will be large. In each case we assign a value to the point $z = 0$, but clearly the values do not correspond to the same situation. In order to prevent the large values of one orientation from drowning out the information contained in the small values from other rotations, we take the minimum of the values assigned to the points z over all rotations.

Let R_θ denote the rotation operator mapping the domain Ω_t^0 onto the rotated domain $R_\theta \Omega_t^0$. If at a point z the value $F(z; \Omega_t^0)$,

$$F(z; \Omega_t^0) := \inf_{\theta \in [0, 2\pi]} f^*(z; R_\theta \Omega_t^0), \tag{3.6}$$

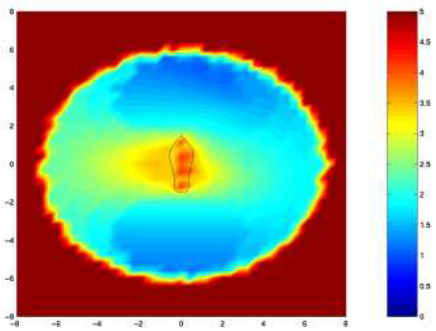

(a)

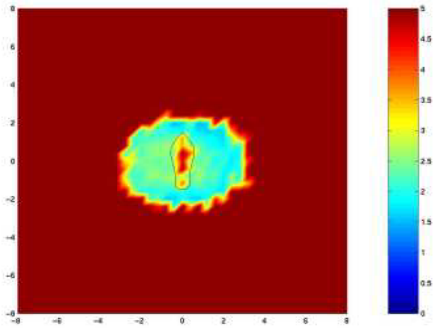

(b)

FIG. 3.2. *The figure demonstrates the calculated corona and the corresponding bound for the location of the unknown obstacle when* Ω_t^0 *is a circle with radius* $r_t = 4$ *as shown in Figure 3.1(a). For this bound we do not need to know the physical nature of the scatterer and only* one *scattered wave is necessary. Here we used the wave number* $\kappa = 5$*, aperture opening* $\theta = 0.9\pi$*;, regularization parameter* $\alpha = 10^{-11}$ *for an incident wave with direction* $(-1, 0)$*. The far field pattern contains 1-2% errors. The figure demonstrates the change in the corona for different choices of the approximation domain: (a) shows the corona for an approximation domain of radius* $r_t = 4$*, (b) shows the corona for an approximation domain of radius* $r_t = 1.3$*.*

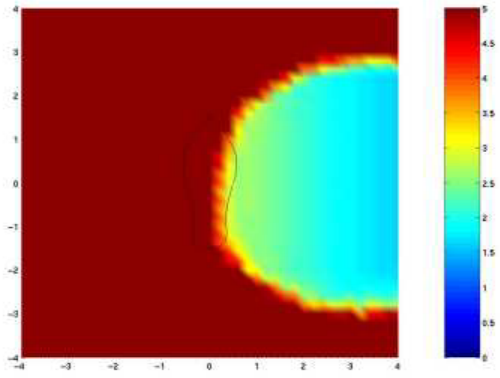

FIG. 3.3. *The figure shows a plot of the function* $f^*(z; \Omega_t^0)$ *given by Eq.(3.5) on a grid containing the unknown scatterer. The scatterer is indicated by the black curve. Here, we used a Dirichlet boundary condition.*

is large, then we suppose that the unknown obstacle lies partly outside all rotations of the test domain about this point. In this way, by sampling all points z in and around the unknown scatterer Ω we are able to reconstruct aspects of the shape, location and size of Ω. Details about how we implement this are given next.

4. Implementation and Numerical demonstrations.

Calculating the densities g. As prescribed in Eq.(3.1), we construct incident fields that are small on the test domain $\Omega_t^0(z)$. For this we approximate the fundamental solution to the Helmholtz equation $\Phi(x,y)$ where the singularity is located at a point $y \in \mathbb{R}^m$ sufficiently far away from $\Omega_t^0(z)$. To construct the densities g corresponding to these incident fields we use Tikhonov regularization to approximately solve the ill-posed equation

$$\Big(H_z g(\cdot,y)\Big)(x) = \Phi(x,y), \quad \text{for } x \in \partial\Omega_t^0(z),$$

where $H_z : L^2(\Gamma) \to L^2(\partial\Omega_t^0(z))$ is a (limited angle) Herglotz wave operator defined by

$$(H_z g)(x) := \int_\Gamma e^{i\kappa x\cdot(-\hat{y})} g(-\hat{y}) ds(\hat{y}), \quad x \in \partial\Omega_t^0(z). \tag{4.1}$$

Specifically, for the regularization parameter $\alpha > 0$, we define

$$g_{z,\alpha}(\cdot,y) := (\alpha I + H_z^* H_z)^{-1} H_z^* \Phi(\cdot,y), \tag{4.2}$$

where the argument y of the density $g_{z,\alpha}$ denotes the dependence of the density on the location of the singularity in Φ. The subscripts z and α on g denote the dependence of the density on the regularization parameter α and the test domain $\Omega_t^0(z)$. This yields

$$v^i[g_{z,\alpha}(\cdot,y)](\cdot) \approx \Phi(\cdot,y) \quad \text{on } \partial\Omega_t^0(z).$$

On $\Omega_t^0(z)$, for $d(y,\Omega_t^0(z)) \geq \rho$ we have, for all $\alpha \in [0,\alpha_0]$ for fixed α_0 sufficiently small,

$$|v^i[g_{z,\alpha}(x,y)]| \leq \begin{cases} \frac{c}{\sqrt{\rho}} & m=2 \\ \frac{c}{\rho} & m=3 \end{cases}, \qquad x \in \Omega_t^0(z), \tag{4.3}$$

with some constant c that is typically of size smaller than 10^1. Thus by knowing the value of $v^i[g_{z,\alpha}]$ at the point closest to the source point we obtain upper bounds on the size of the incident field on all of $\Omega_t^0(z)$. This is used in the calculation of the scattering test response μ_ϵ. On the exterior region $\mathbb{R}^m \backslash \overline{\Omega}_t$ the magnitude of $v^i[g_{z,\alpha}]$ is in the range of $c/2\alpha$. For example $|v^i[g_{z,\alpha}]|$ is of size 50 if $c = 1$ and $\alpha = 10^{-2}$. This corresponds to a data error of one percent.

Translations of the test domain. We describe a quick method to calculate lower estimates for the test response μ_ϵ for a large number of translated test domains $\Omega_t^0(z)$ with generating domain Ω_t^0. In the moving reference frame of the test domain, spatial translations look like translations of the incident field. We use this and the fact that phase shifts in the far field correspond to spatial translations in the near field in order to translate the generating domain Ω_t^0 around the computational domain.

Let Ω_t^0 be a generating test domain and define $\Omega_t^0(z) = \Omega_t^0 + z$ to be the corresponding translated test domain. Translations of the Herglotz wave function $v^i[g]$ can be easily performed by the multiplication of the density g by the complex factor $e^{-i\kappa z\cdot d}$. At points $z \in \mathbb{Q}$ covering the area where the unknown scatterer is supposed to be (that is, $\mathbb{Q}$ is the computational domain

and satisfies $\Omega \subset \mathbb{Q}$) we calculate translations $\Omega_t^0(z)$ of the test domain Ω_t^0 by the corresponding translation of the Herglotz wave function $v^i[g]$:

$$v^i[g](x-z) = v^i[e^{-i\kappa z\cdot(\cdot)}g(\cdot)](x), \quad x \in \mathbb{R}^m. \tag{4.4}$$

We define the function $|v^\infty[g](\hat{x},z)|$ to be the far field pattern at the point $\hat{x} \in \mathbb{S}$ for scattering of the shifted incident field $v^i[g](x-z)$. Then from Theorem 2.1 and Eq.(3.2) we obtain

$$|v^\infty[g](\hat{x},z)| = \Big| \int_\Gamma u^\infty(\hat{y},-\hat{x}) e^{i\kappa z\cdot\hat{y}} g(-\hat{y}) ds(\hat{y}) \Big|. \tag{4.5}$$

In words, the magnitude of the far field v^∞ at the point $\hat{x} \in \mathbb{S}$ with test domain $\Omega_t^0(z)$ is given by the magnitude of the weighted superposition of the measured far field pattern due to a single incident plane wave excitation; the weight $g(-\hat{y})$ is determined by the generating domain Ω_t^0 and the phase shift is determined by the translation of Ω_t^0.

Sampling the scattering test response. The scattering test response $\mu_\epsilon(\Omega_t^0(z),\Omega)$ is the supremum over $|v^\infty[g](\hat{x},z)|$ where $g \in L^2(\Gamma)$ is chosen such that

$$||v^i[g]||_{C(\Omega_t^0(z))} \leq \epsilon. \tag{4.6}$$

We choose a finite subset $\{g_1,\ldots,g_{n_y}\}$ of densities g such that (4.6) is satisfied and calculate the maximum of the values $|v^\infty[g_j](\hat{x},z)|$ for $j=1,\ldots,n_y$ via Eq.(4.5). To obtain different densities g we solve Eq.(4.2) at the points y_j, $j=1,\ldots,n_y$ in the exterior of $\Omega_t^0(z)$. In our experiments we chose $n_y \approx 20$. Using the efficient translations in Eq.(4.4), we need only solve Eq.(4.2) for g with Ω_t^0 for each $j=1,\ldots,n_y$, rather than solving for g for every translated domain $\Omega_t^0(z)$. Also, from the discussion following Eq.(4.3) if we choose the points y_j appropriately, there is no need to check explicitly if condition Eq.(4.6) is satisfied.

The no response algorithm We finish this section with a detailed prescription for using the no response test to locate an unknown obstacle.

ALGORITHM 4.1 (no response test).

- *Choose an appropriate test domain Ω_t^0 with $0 \in \partial\Omega_t^0$, that is large enough such that translations of Ω_t^0 and its rotated versions may contain the unknown scatterer (see Figure 3.1).*
- *For the angles $\theta_l := 2\pi l/n_r$ with $l=1,\ldots,n_r$ let $R_{\theta_l}\Omega_t^0$ be the domain that is obtained from Ω_t^0 by rotation around the origin by angle θ_l as described in Section 3. For each $l=1,\ldots,n_r$ do:*
  - *Choose points y_j, $j=1,\ldots,n_y$ in the exterior of $R_{\theta_l}\Omega_t^0$ and calculate the density $g_{l,j}$ by*

$$g_{l,j} := (\alpha I + H_{\theta_l}^* H_{\theta_l})^{-1} H_{\theta_l}^* \Phi(\cdot, y_j)$$

    where H_{θ_l} is the Heglotz wave operator (see Eq.(4.1)) corresponding to the rotated domain $R_{\theta_l}\Omega_t^0$.
  - *For each $j=1,\ldots,n_y$ calculate*

$$f_j(z; R_{\theta_l}\Omega_t^0) := \Big| \int_\Gamma u^\infty(\hat{y},-\hat{x}) e^{i\kappa z\cdot\hat{y}} g_{l,j}(-\hat{y}) ds(\hat{y}) \Big|,$$

    for all $z \in \mathcal{G}$, the computational grid, from the one-wave far field pattern $u^\infty(\hat{y},-\hat{x})$, $\hat{y} \in \Gamma$.

– *Calculate the maximum with respect to the densities $g_{l,j}$, that is calculate the sampled version of Eq.(3.5)*

$$f^*(z; R_{\theta_l}\Omega_t^0) := \max_{j=1,\dots,n_y} f_j(z; R_{\theta_l}\Omega_t^0), \quad z \in \mathcal{G}.$$

- *Calculate the minimum with respect to the rotations θ_l, that is the sampled version of Eq.(3.6):*

$$F(z; \Omega_t^0) := \min_{l=1,\dots,n_r} f^*(z; R_{\theta_l}\Omega_t^0), \quad z \in \mathcal{G}.$$

- *Choose a threshold C and calculate*

$$\Omega_{rec} := \big\{ z \in \mathcal{G} : \quad F(z; \Omega_t^0) \geq C \big\}.$$

Now, an approximation for the support Ω of the unknown scatterer is given by the components of Ω_{rec} that are not connected with infinity.

For the choice of the constant C we propose dynamical thresholding on the image $F(z)$ that is informed by a priori knowledge about the approximate size of the object.

Numerical results. All the following numerical reconstruction procedures are based on the same algorithm independent of the boundary condition or physical nature of the scatterer. All reconstructions use the far field data for *one* wave only. We show results for full and limited aperture data.

To compare different reconstructions for obstacles with different boundary condition for all the following pictures we used the far field pattern for one wave with direction of incidence $(-1, 0)$. We first show results for full aperture and demonstrate the influence of the cut-off parameter.

In a second part, we restrict our measurements to a limited aperture. Here, we would like to show that even with limited aperture the method yields reasonable results. Figures 4.7 to 4.10 show limited aperture reconstructions for the Dirichlet, Neumann and impedance boundary condition and for the inhomogeneous medium. We used $\kappa = 5$ and an aperture of 0.6π, or $108°$.

5. Concluding remarks. The no response test is a novel sampling technique for reconstructing the support of unknown scatterers. The method does not require a priori knowledge about the physical or geometric properties of the unknown scatterer. Reconstructions can be obtained from the far field pattern for scattering of a single incident wave. The method appears to be robust and can be used in limited aperture settings. The results and open questions discussed in this work offer a new perspective on some old questions (for example the uniqueness question for one wave) and provide new directions for future research, both in numerical techniques and analysis.

REFERENCES

[1] Colton, D. and Kirsch, A.: "A simple method for solving inverse scattering problems in the resonance region." *Inverse problems* **12**(4), 383-93 (1996).

[2] Colton, D. and Kress, R.: *Inverse Acoustic and Electromagnetic Scattering Theory.* 2nd Ed., Springer-Verlag (1998).

[3] Colton, D. and Monk, P.: "A novel method for solving the inverse scattering problem for time-harmonic waves in the resonance region." *SIAM J. Appl. Math.* **45**, 1039-1053 (1985).

[4] Colton, D. and Monk, P.: "A novel method for solving the inverse scattering problem for time-harmonic waves in the resonance region II." *SIAM J. Appl. Math.* **46**, 506-523 (1986).

[5] Colton, D. and Sleeman, B. D.: "Uniqueness theorems for the inverse problem of acoustic scattering." *IMA J. Appl. Math.* **31**, 253-259 (1983).

[6] Ikehata, M.: "Reconstruction of an obstacle from the scattering amplitude at a fixed frequency." Inverse Problems 14 (1998), no. 4, 949–954.

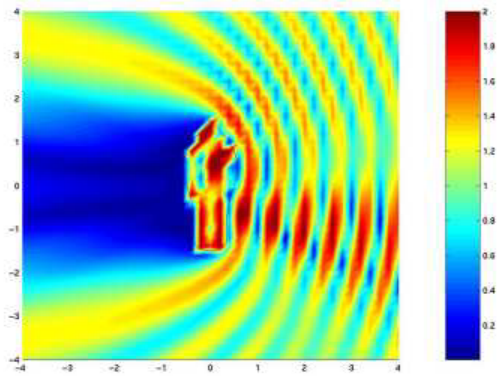

(a)

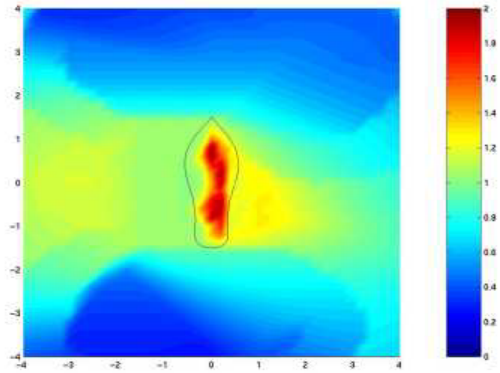

(b)

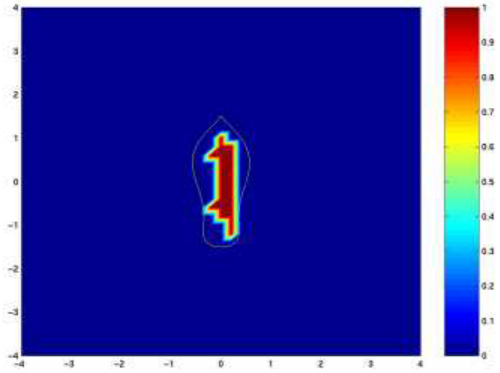

(c)

FIG. 4.1. *(a) Original total field for scattering by a Dirichlet obstacle. (b) A plot of the function $F(z)$ defined by (3.6) for $z \in \mathcal{G}$, the computational grid. (c) Thresholded version of the function F with $C = 1.4$ (see Alg. 4.1). Here we used the wave number $\kappa = 5$, aperture opening $\theta = 1.8\pi$;, regularization parameter $\alpha = 10^{-11}$ for an incident wave with direction $(-1, 0)$. The far field pattern contains 1-2% errors.*

[7] Ikehata, M.: "Enclosing a polygonal cavity in a two-dimensional bounded domain from Cauchy data", Inverse Problems 15 (October 1999) 1231-1241.
[8] Ikehata, M.: "On reconstruction in the inverse conductivity problem with one measurement", Inverse Problems 16 (2000) 785-793.
[9] Ikehata, M. and Ohe, T.: "A numerical method for finding the convex hull of polygonal cavities using the enclosure method", Inverse Problems 18 (2002) 111-124.
[10] Kirsch, A: "Characterization of the shape of a scattering obstacle using the spectral data of the far field operator." *Inverse problems* **14**(6), 1489-1512 (1998).
[11] Lies, R.: *Initial Boundary Value Problems in Mathematical Physics,* B.G. Teubner, Stuttgart (1985).
[12] Mitrea, D., Mitrea, M., Taylor, M.: " Layer potentials, the Hodge Laplacian, and global boundary problems in nonsmooth Riemannian manifolds", *Mem. Amer. Math. Soc.* **150**(2001).
[13] Panich, O.I.:, "On the question of the solvability of the exterior boundary-value problems for the wave equation and Maxwell's equations. Usp. Mat Nauk **20A**, 221-226 (1965) (Russian).
[14] Potthast, R.: "A fast new method to solve inverse scattering problems." Inverse Problems 12, 731-742 (1996).
[15] Potthast, R.: "A point-source method method for inverse acoustic and electromagnetic obstacle scattering problems." IMA Jour. Appl. Math. 61, 119-140 (1998).
[16] Potthast, R.: *Point sources and multipoles in inverse scattering theory.* Chapman & Hall (2001).

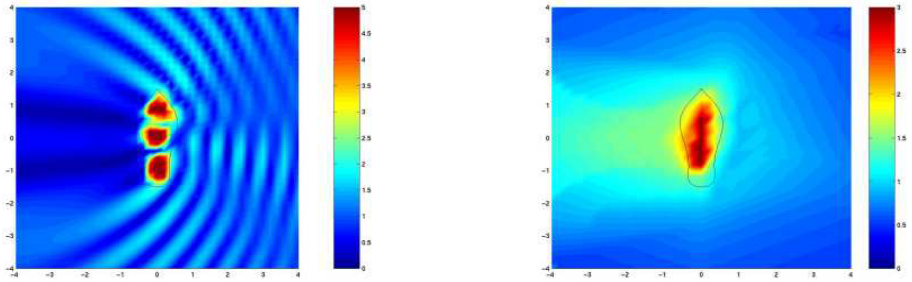

(a) (b)

FIG. 4.2. *(a) Original total field for scattering by an impedance obstacle with $\lambda = i$. (b) A plot of the function $F(z)$ defined by (3.6) for $z \in \mathcal{G}$, the computational grid. Here we used the wave number $\kappa = 5$, aperture opening $\theta = 1.8\pi$;, regularization parameter $\alpha = 10^{-11}$ for an incident wave with direction $(-1, 0)$. The far field pattern contains 1-2% errors.*

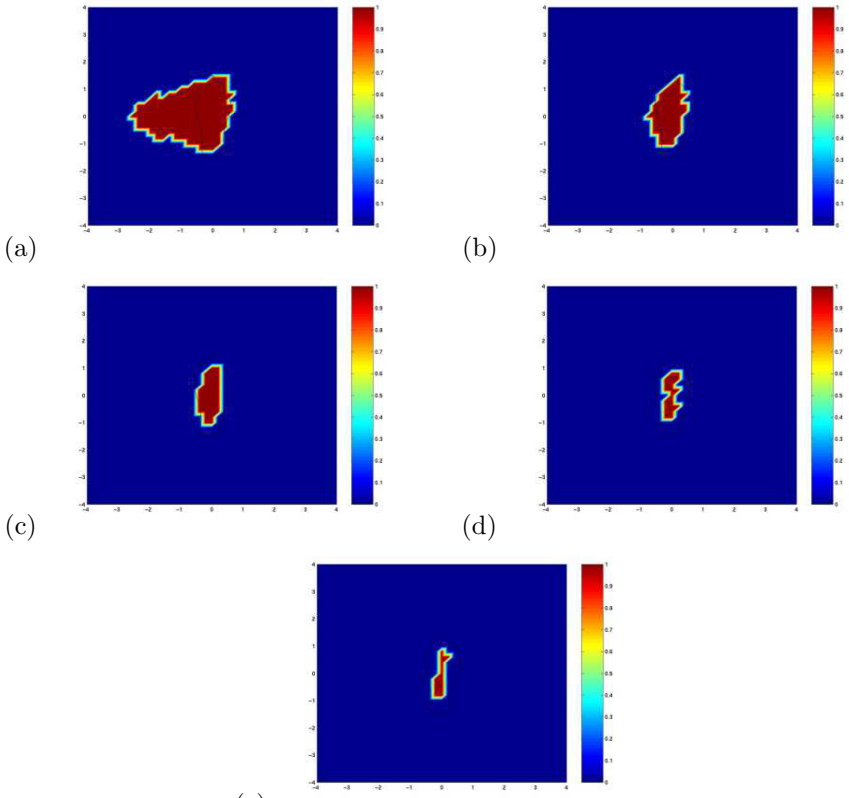

(a) (b) (c) (d) (e)

FIG. 4.3. *We show different thresholded versions of the reconstruction to demonstrate the influence of the cut-off parameter C. The wave number is $\kappa = 5$, aperture opening $\theta = 1.8\pi$;, regularization parameter $\alpha = 10^{-11}$ for an incident wave with direction $(-1, 0)$, that is the incident wave is coming from the right-hand side. The far field pattern contains 1-2% errors.*

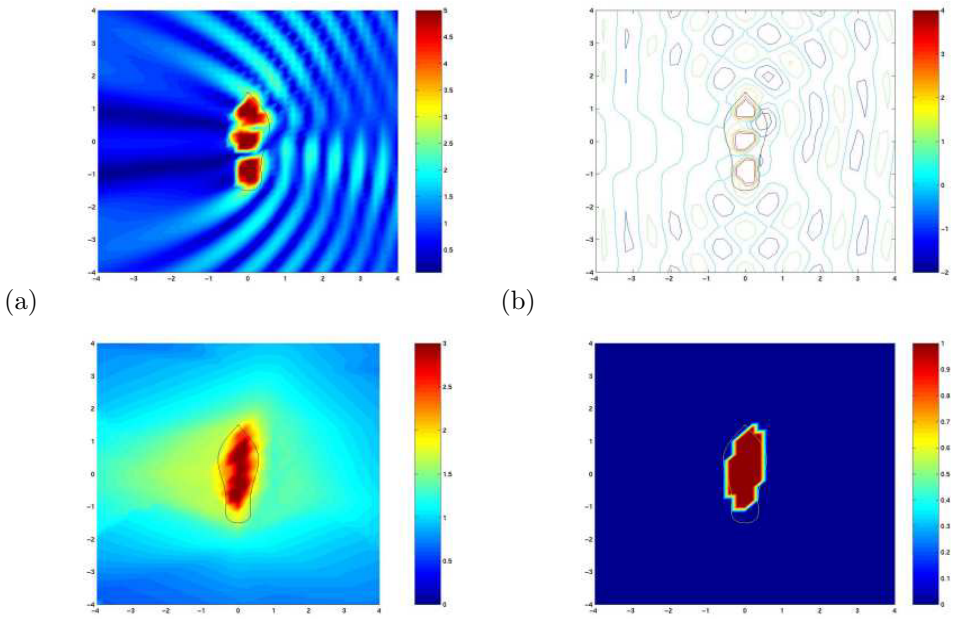

(a) (b)

(c) (d)

FIG. 4.4. *(a)-(b) Original total field for scattering by an obstacle with Neumann boundary condition, we show a surface and a contour plot of the field. (c) A plot of the function $F(z)$ defined by (3.6) for $z \in \mathcal{G}$ and (d) a thresholded version of the reconstruction with $C = 2.0$. Here we used the wave number $\kappa = 5$, aperture opening $\theta = 1.8\pi$;, regularization parameter $\alpha = 10^{-11}$ for an incident wave with direction $(-1, 0)$. The far field pattern contains 1-2% errors.*

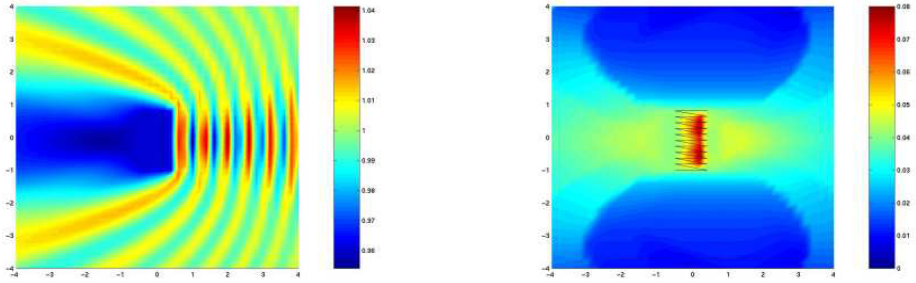

(a) (b)

FIG. 4.5. *(a) Original total field for scattering by a homogeneous penetrable medium with $n := 4$ in Ω where the inhomogeneity is shown in Figure 3.1. (b) A plot of the function $F(z)$ defined by (3.6) for $z \in \mathcal{G}$. Here we used the wave number $\kappa = 5$, aperture opening $\theta = 1.8\pi$;, regularization parameter $\alpha = 10^{-11}$ for an incident wave with direction $(-1, 0)$. The far field pattern contains 1-2% errors.*

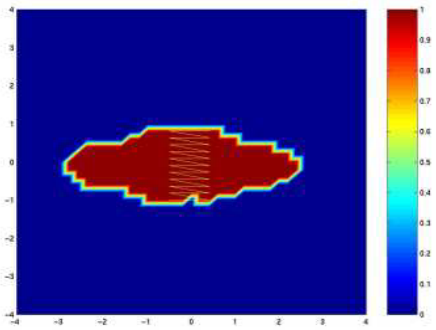

(a)

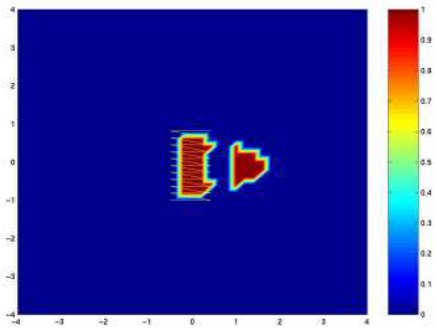

(b)

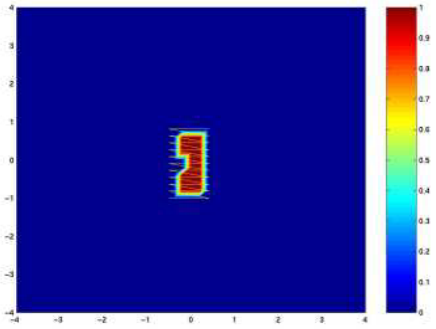

(c)

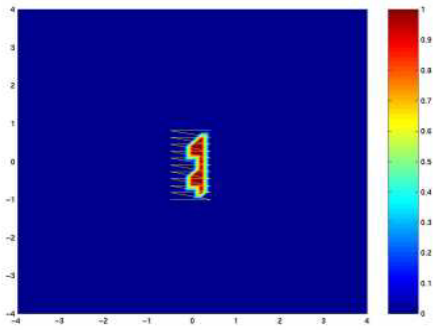

(d)

FIG. 4.6. *(a)-(d) We show several thresholded versions of the function F for the reconstruction of an inhomogeneous medium, where we used the thresholds $C = 0.1$, $C = 0.06$ $C = 0.05$ and $C = 0.045$.*

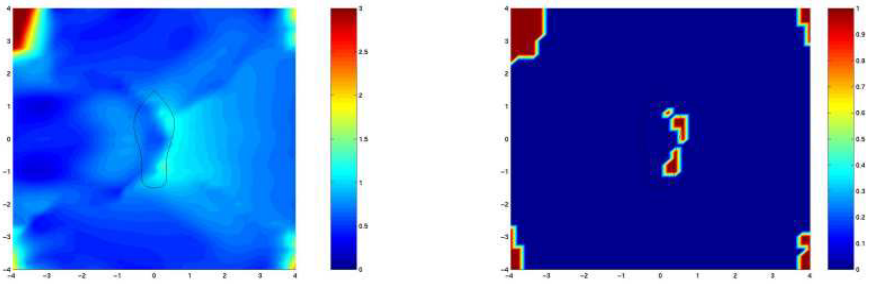

(a) (b)

FIG. 4.7. *Limited aperture reconstruction of a Dirichlet obstacle. (a) A plot of the function $F(z)$ defined by (3.6) for $z \in \mathcal{G}$, the computational grid. (b) Thresholded version of the function F. Here we used the wave number $\kappa = 5$, aperture opening $\theta = 0.6\pi$;, regularization parameter $\alpha = 10^{-11}$ for an incident wave with direction $(-1, 0)$. The far field pattern contains 1-2% errors.*

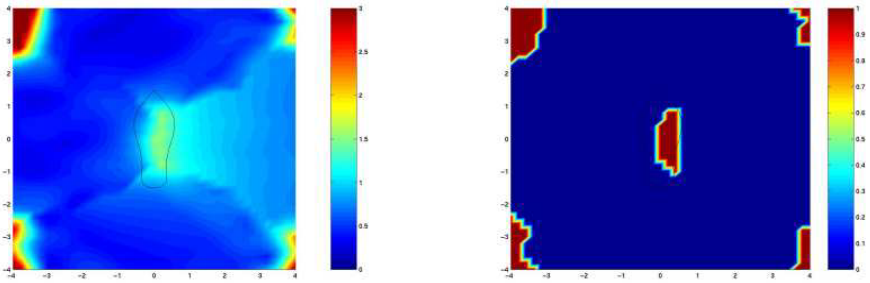

(a) (b)

FIG. 4.8. *Limited aperture reconstruction of a Neumann obstacle. (a) A plot of the function $F(z)$ defined by (3.6) for $z \in \mathcal{G}$. (b) Thresholded version of the function F. Here we used the wave number $\kappa = 5$, aperture opening $\theta = 0.6\pi$;, regularization parameter $\alpha = 10^{-11}$ for an incident wave with direction $(-1, 0)$. The far field pattern contains 1-2% errors.*

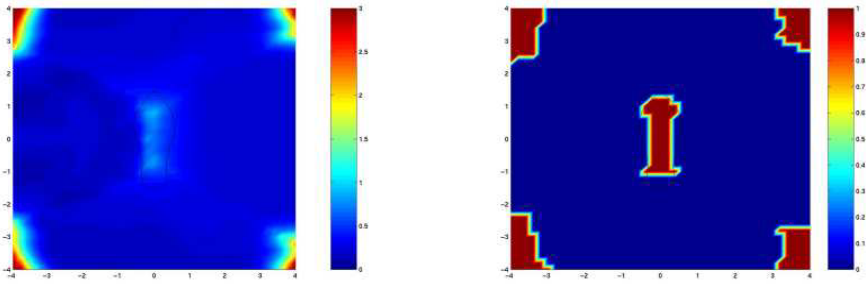

(a) (b)

FIG. 4.9. *Limited aperture reconstruction of an impedance obstacle with $\lambda = i$. (b) A plot of the function $F(z)$ defined by (3.6) for $z \in \mathcal{G}$, the computational grid. (c) Thresholded version of the function F. Here we used the wave number $\kappa = 5$, aperture opening $\theta = 0.6\pi$;, regularization parameter $\alpha = 10^{-11}$ for an incident wave with direction $(-1, 0)$. The far field pattern contains 1-2% errors.*

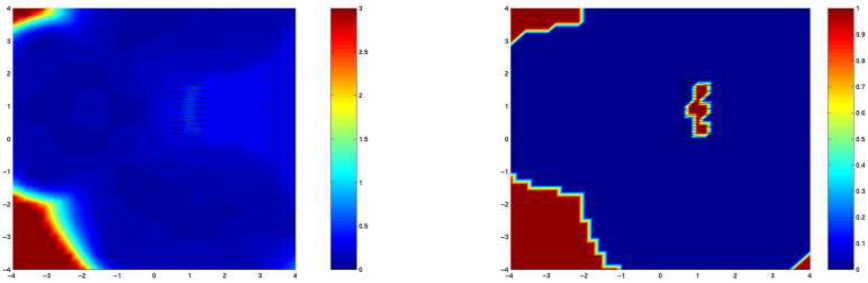

(a) (b)

FIG. 4.10. *Limited aperture reconstruction of the support of an inhomogeneous medium. (a) A plot of the function $F(z)$ defined by (3.6) for $z \in \mathcal{G}$. (b) Thresholded version of the function F. Here we used the wave number $\kappa = 5$, aperture opening $\theta = 0.6\pi$;, regularization parameter $\alpha = 10^{-11}$ for an incident wave with direction $(-1, 0)$. The far field pattern contains 1-2% errors.*